Table 1
Inhibition of AKR1B10 and AKR1B1 by the **1**-based derivatives

Compound	IC_{50} (nM)		Ratio [a]
	AKR1B10	AKR1B1	
1	6.0 ± 0.1	11 ± 1.0	1.8
5a	6.8 ± 0.3	24 ± 1.1	3.5
5b	7.6 ± 1.0	19 ± 1.3	2.5
5c	8.6 ± 0.8	26 ± 3.0	3.0
5d	14 ± 0.8	25 ± 4.4	1.8
5e	13 ± 2.1	12 ± 1.5	0.9
5f	13 ± 1.6	20 ± 2.4	1.5
5g	12 ± 2.3	34 ± 1.5	2.8
5h	9.7 ± 1.6	6.7 ± 0.4	0.7
5i	18 ± 3.3	28 ± 2.7	1.6
5j	16 ± 2.1	28 ± 3.3	1.8
5k	11 ± 0.5	27 ± 4.6	2.5
5l	11 ± 0.5	20 ± 1.1	1.8
5m	8.8 ± 1.0	29 ± 0.4	3.3
5n	4.7 ± 0.04	24 ± 2.4	5.1
5o	>10,000 [b]	>10,000[b]	–
5p	>10,000[b]	>10,000[b]	–
5q	290 ± 30	>10,000[b]	–
5r	>10,000[b]	>10,000[b]	–

[a] Selectivity is expressed as a ratio of AKR1B1/AKR1B10.
[b] Inhibition percentages are less than 30% at 10,000 nM.

2.2. Biological evaluation and SAR of 5

Newly synthesized compounds (**5**), except for **5o–r,** showed potent inhibition for AKR1B10, with less than 3-fold increases in the IC_{50} values compared with that of the original compound **1** (Table 1). While the replacement of the 4-methoxy group on the 2-phenylimino moiety of **1** with halogen (**5d**, **5e**) or CH_2CO_2H group (**5f**) slightly decreased the inhibitory potency, that with OH (**5a**), CO_2H (**5b**) or Me group (**5c**) had apparently no significant effect. This indicates that the 4-methoxy group is not an essential structural prerequisite for the tight binding of **1**, which is suggested by the previous dock model.[18] With respect to the moiety bound to the carboxyamide of the chromene ring, small alkyls (less than 3 carbons) or Bn substituent are better than *c*-Hex, *n*-Bu, or *i*-Bu as the substituent on the amide nitrogen. Among the synthesized compounds, the Bn derivative (**5n**) was the most potent and selective inhibitor of AKR1B10 (IC_{50} = 4.7 nM). The inhibition pattern of **5n** was competitive with respect to the alcohol substrate, geraniol, of AKR1B10, and its K_i value was 1.3 ± 0.3 nM (Fig. 2), which is the lowest among the values of the known inhibitors.[10,11,13,14,17,18] In contrast, the removal of the 7-hydroxyl group on the chromene ring (**5o–r**) resulted in drastic decreases in inhibitory potency, suggesting a crucial role of the 7-hydroxyl group in the tight binding of **1** to AKR1B10.

2.3. Docking model of 5n in AKR1B10

The above SAR studies of 2-phenyliminochromene derivatives (**5a–r**) revealed that the 7-hydroxyl group on the chromene ring is an essential moiety for their potent inhibition of AKR1B10. The underlying structural reasons for the high affinity of the 7-hydroxy-chromene derivatives were examined by constructing a model of docked **5n** in the AKR1B10-$NADP^+$ complex (Fig. 1B). In this model, **5n** occupied the substrate-binding site of the enzyme, in which its 7-hydroxyl group formed hydrogen-bond interactions with the catalytically important residues, Tyr49 and His111 (2.9 Å and 3.0 Å, respectively), and the chromene ring was surrounded by hydrophobic residues (Trp21, Val48, Trp112, and Trp220). An additional hydrogen-bond interaction between the oxygen in the chromene ring and the side chain of Trp21 (3.1 Å) was suggested. The orientation of the chromene ring of **5n** is contrast to that in the previous **1**-docked model (Fig. 1A), in which the 7-hydroxy-chromene ring is oppositely positioned. The benzylamide moiety of **5n** formed a π-stacking interaction with the side chain of Trp220 (3.5 Å), which may account for the higher inhibitory potency for AKR1B10 than other derivatives with alkylamide and *c*-hexylamide moieties (**5h–m**). In fact, the

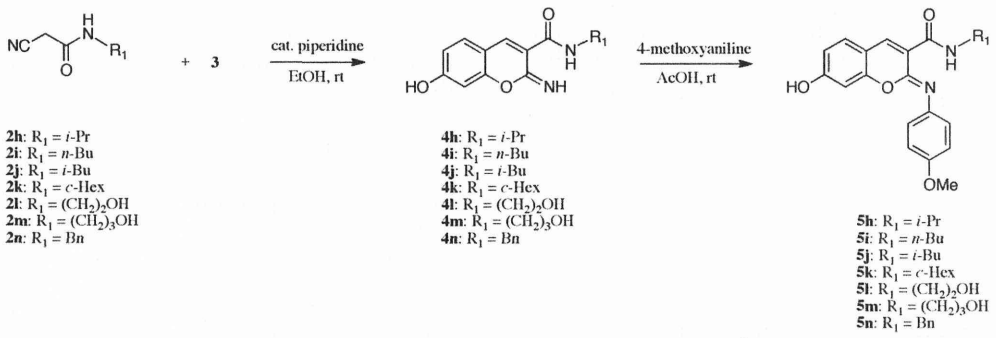

Scheme 2. Synthesis of chromene derivatives **5h–n**.

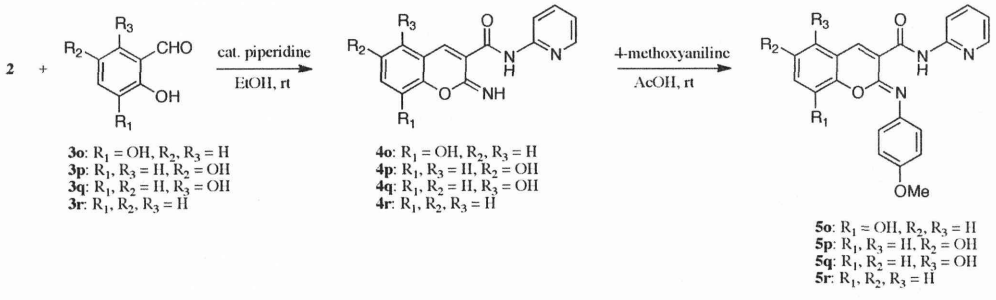

Scheme 3. Synthesis of chromene derivatives **5o–r**.

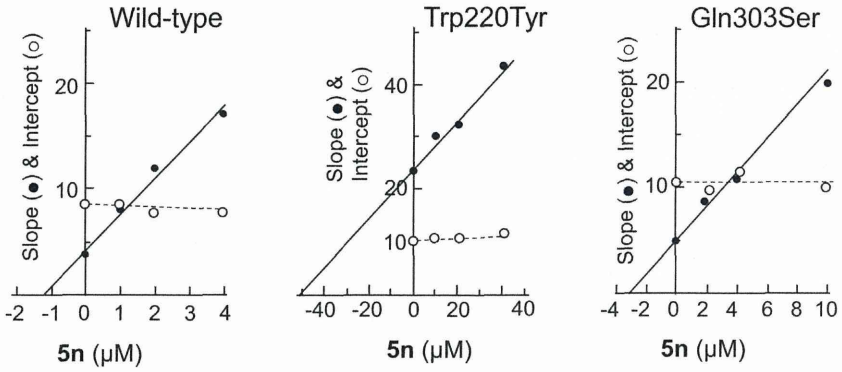

Figure 2. Inhibition of wild-type and mutant AKR1B10s by **5n**. The activity was determined with 0.25 mM $NADP^+$ and geraniol (25–200 μM for the wild-type and Gln303Ser enzymes; and 50–800 μM for Trp220Tyr enzyme) in the presence of the indicated concentrations of **5n**. The velocities were plotted double-reciprocally versus the substrate concentrations, and replots of the slopes (μM mL munit^{-1}) and intercepts (munit mL^{-1} × 10^2) versus the inhibitor concentrations are shown in the figure.

Trp220Tyr mutagenesis of the enzyme resulted in a 39-fold increase in the K_i value for **5n** (51.0 ± 1.0 nM) compared to that determined with the wild-type enzyme (Fig. 2). The benzylamide moiety of **5n** is also close to the side-chain of Gln303 (3.3 Å), which corresponds to Ser in AKR1B1, and the mutation of Gln303Ser decreased the affinity for **5n** (K_i = 3.8 ± 0.1 nM, Fig. 2) by 3-fold. Gln303 might be related to the highest AKR1B10-inhibitory selectivity of **5n** among the derivatives. The 4-methoxy group on the 2-phenylimino moiety of **5n** was located in the external region of the substrate-binding pocket, in which only the side-chain of Gln50 was close to the 4-methoxy group. This orientation may explain the insignificant alteration in the inhibitory potency following the replacement of the 4-methoxy group (**5a–g**).

3. Conclusion

In this study, a series of 2-phenyliminochromene derivatives (**5a–r**) were synthesized, and their inhibitory activities for AKR1B10 were evaluated. The SAR of the synthesized compounds revealed that the hydroxyl group on the chromene ring at the 7-position was essential to maintain the potent inhibitory effect. The necessity of the 7-hydroxyl group was in agreement with the molecular docking model of **5n** in complex with AKR1B10–$NADP^+$, in which the 7-hydroxyl group forms strong hydrogen bond interactions with catalytically important residues, Tyr49 and His111, of the active site of the enzyme.

4. Experimental section

4.1. Chemistry

4.1.1. General procedure for Knoevenagel condensation

To a stirred solution of cyanamide (**2**, 1.1 mmol) in ethanol (2 mL) were added 2-hydroxybenzaldehyde (1 mmol) and piperidine (catalytic amount), and the resulting mixture was stirred at room temperature for 12 h. The suspension was then filtered to give **4**, which was used directly in the next step.

4.1.1.1. 7-Hydroxy-2-imino-2*H*-chromene-3-carboxylic acid pyridin-2-ylamide (4). Yield: 88%; ^{1}H NMR (400 MHz, DMSO-d_6) δ 6.59 (1H, s), 6.71 (1H, d, J = 8.5 Hz), 7.13 (1H, t, J = 8.9 Hz), 7.64 (1H, d, J = 8.5 Hz), 7.83 (1H, t, J = 8.9 Hz), 8.25 (1H, d, J = 8.9 Hz), 8.31–8.32 (1H, m), 8.50 (1H, s), 9.02 (1H, br), 13.14 (1H, s).

4.1.1.2. 7-Hydroxy-2-imino-2*H*-chromene-3-carboxylic acid isopropylamide (4h). Yield: 45%; ^{1}H NMR (400 MHz, DMSO-d_6) δ 1.17 (6H, s), 4.05 (1H, sept, J = 6.5 Hz), 6.78 (1H, s), 6.86 (1H, dd, J = 1.3, 7.3 Hz), 7.89 (1H, dd, J = 1.3, 7.3 Hz), 8.44–8.45 (1H, m), 8.76 (1H, br), 11.02 (1H, br).

4.1.1.3. 7-Hydroxy-2-imino-2*H*-chromene-3-carboxylic acid butylamide (4i). Yield: 61%; ^{1}H NMR (400 MHz, $CDCl_3$) δ 0.95 (3H, t, J = 7.1 Hz), 1.41 (2H, sext, J = 7.1 Hz), 1.60 (2H, quint, J = 7.1 Hz), 3.42 (2H, t, J = 7.1 Hz), 6.64 (1H, s), 6.72 (1H, dd, J = 2.4, 5.9 Hz), 7.33 (1H, d, J = 8.3 Hz), 8.81 (1H, s).

4.1.1.4. 7-Hydroxy-2-imino-2*H*-chromene-3-carboxylic acid isobutylamide (4j). Yield: 49%; ^{1}H NMR (400 MHz, DMSO-d_6) δ 0.94 (6H, d, J = 6.6 Hz), 1.81 (1H, m), 2.08 (2H, d, J = 6.6 Hz), 6.64 (1H, s), 6.72 (1H, dd, J = 2.4, 5.9 Hz), 7.33 (1H, d, J = 8.3 Hz), 8.81 (1H, s).

4.1.1.5. 7-Hydroxy-2-imino-2*H*-chromene-3-carboxylic acid cyclohexylamide (4k). Yield: 68%; ^{1}H NMR (400 MHz, DMSO-d_6) δ 1.25–1.97 (10H, m), 3.95 (1H, quint, J = 7.8 Hz), 6.64(1H, s), 6.73 (1H, dd, J = 2.4, 6.2 Hz), 7.30 (1H, d, J = 8.6 Hz), 8.35 (1H, s), 10.03 (1H, br).

4.1.1.6. 7-Hydroxy-2-imino-2*H*-chromene-3-carboxylic acid (2-hydroxyethyl)amide (4l). Yield: 81%; ^{1}H NMR (400 MHz, DMSO-d_6) δ 3.25 (2H, t, J = 7.1 Hz), 3.46 (2H, t, J = 7.1 Hz), 4.77 (1H, br), 6.53 (1H, s), 6.65 (1H, d, J = 8.5 Hz), 7.55 (1H, d, J = 8.5 Hz), 8.3 (1H, s), 10.33 (1H, br).

4.1.1.7. 7-Hydroxy-2-imino-2*H*-chromene-3-carboxylic acid (3-hydroxypropyl)amide (4m). Yield: 43%; ^{1}H NMR (400 MHz, DMSO-d_6) δ 1.62 (2H, quint, J = 6.5 Hz), 3.29 (2H, t, J = 6.5 Hz), 3.38 (2H, t, J = 6.5 Hz), 4.10 (1H, br), 6.54 (1H, s), 6.66 (1H, dd, J = 2.1, 6.2 Hz), 7.55 (1H, d, J = 8.3 Hz), 8.29 (1H, s), 8.74 (1H, br), 10.24 (1H, br), 10.63 (1H, br).

4.1.1.8. 7-Hydroxy-2-imino-2*H*-chromene-3-carboxylic acid benzylamide (4n). Yield: 98%; ^{1}H NMR (400 MHz, DMSO-d_6) δ 4.50 (2H, d, J = 5.9 Hz), 6.55 (1H, dd, J = 2.2, 6.3 Hz), 7.23–7.35 (5H, m), 7.56 (1H, d, J = 8.5 Hz), 8.42 (1H, s), 10.66 (1H, br).

4.1.1.9. 8-Hydroxy-2-imino-2*H*-chromene-3-carboxylic acid pyridin-2-ylamide (4o). Yield: 78%; ^{1}H NMR (400 MHz, DMSO-d_6) δ 7.07–7.24 (4H, m), 7.83 (1H, t, J = 7.5 Hz), 8.26 (1H, d, J = 8.5 Hz), 8.33 (1H, d, J = 7.5 Hz), 8.54 (1H, s), 9.14 (1H, br), 10.22 (1H, br), 13.26 (1H, br).

4.1.1.10. 6-Hydroxy-2-imino-2*H*-chromene-3-carboxylic acid pyridin-2-ylamide (4p). Yield: 86%; ^{1}H NMR (400 MHz, DMSO-d_6) δ 6.99–7.17 (4H, m), 7.84 (1H, t, J = 8.4 Hz), 8.25 (1H, d,

J = 8.4 Hz), 8.3–8.34 (1H, m), 8.52 (1H, s), 9.06 (1H, br), 9.74 (1H, br).

4.1.1.11. 5-Hydroxy-2-imino-2*H*-chromene-3-carboxylic acid pyridin-2-ylamide (4q). Yield: 81%; ^{1}H NMR (400 MHz, DMSO-d_6) δ 6.36 (1H, d, J = 7.9 Hz), 6.49 (1H, d, J = 8.4 Hz), 7.12 (1H, t, J = 8.4 Hz), 7.24 (1H, t, J = 7.9 Hz), 7.80 (1H, t, J = 7.9 Hz), 8.26–8.32 (2H, m), 13.19 (1H, br).

4.1.1.12. 2-Imino-2*H*-chromene-3-carboxylic acid pyridin-2-ylamide (4r). Yield: 89%; ^{1}H NMR (400 MHz, DMSO-d_6) δ 7.04–7.27 (4H, m), 7.48–7.55 (2H, m), 7.74 (1H, t, J = 7.9 Hz), 8.36–8.39 (2H, m), 8.57 (1H, s), 13.09 (1H, br).

4.1.2. General procedure for synthesis of compounds (5a–r)

To a stirred solution of chromene (**4**, 1 mmol) in acetic acid (2 mL) was added aniline (1 mmol), and the resulting mixture was stirred at room temperature for 12 h. The solvent was removed under reduced pressure, and the residue was chromatographed on silica gel to give **5** as the yellow solid.

4.1.2.1. 7-Hydroxy-2-(4-hydroxyphenylimino)-2*H*-chromene-3-carboxylic acid pyridin-2-ylamide (5a: R = OH). Yield: 52%; mp: >300 °C; ^{1}H NMR (400 MHz, DMSO-d_6) δ 6.62 (1H, s), 6.74 (1H, dd, J = 2.2, 6.1 Hz), 6.82 (2H, t, J = 8.8 Hz), 7.14 (1H, t, J = 7.6 Hz), 7.33 (2H, d, J = 8.8 Hz), 7.65 (1H, d, J = 8.3 Hz), 7.83 (1H, t, J = 7.6 Hz), 8.27 (1H, d, J = 7.6 Hz), 8.36–8.36 (1H, m), 8.54 (1H, br); ^{13}C NMR (100 MHz, DMSO-d_6) δ 100.11, 101.54, 110.94, 113.26, 113.69, 115.45, 115.95, 119.84, 125.24, 131.58, 134.89, 138.44, 147.58, 148.52, 151.62, 154.85, 154.98, 160.48, 163.15; IR (neat): 3312, 1661, 1574, 1506, 1437 cm^{-1}; IR (KBr): 3396, 1666, 1591, 1549, 1435 cm^{-1}; MS (EI): m/z 373 (M$^+$); HRMS: Calcd for $C_{21}H_{15}N_3O_4$ 373.1063. Found 373.1060.

4.1.2.2. 4-[7-Hydroxy-3-(pyridin-2-ylcarbamoyl)-chromen-2-ylideneamino]-benzoic acid (5b: R = CO_2H). Yield: 34%; mp: >300 °C; ^{1}H NMR (400 MHz, DMSO-d_6) δ 6.51 (1H, s), 6.76 (1H, dd, J = 2.4, 6.1 Hz), 7.14 (1H, t, J = 7.8 Hz), 7.38 (2H, d, J = 8.6 Hz), 7.71 (1H, d, J = 7.8 Hz), 7.84 (1H, t, J = 7.8 Hz), 7.99 (2H, d, J = 8.6 Hz), 8.28–8.35 (2H, m), 8.68 (1H, s), 12.73 (1H, br); ^{13}C NMR (100 MHz, DMSO-d_6) δ 72.73, 93.77, 101.47, 111.00, 113.74, 115.35, 119.96, 123.09, 130.40, 131.89, 138.50, 143.72, 148.29, 148.47, 150.23, 151.45, 154.91, 160.30, 163.60, 167.17; IR (KBr): 3422, 1680, 1589, 1437 cm^{-1}; MS (EI): m/z 401 (M$^+$); HRMS: Calcd for $C_{22}H_{15}N_3O_5$ 401.1012. Found 401.1013.

4.1.2.3. 7-Hydroxy-2-*p*-tolylimino-2*H*-chromene-3-carboxylic acid pyridin-2-ylamide (5c: R = Me). Yield: 47%; mp: >300 °C; ^{1}H NMR (400 MHz, DMSO-d_6) δ 2.33 (1H, s), 6.76 (1H, dd, J = 2.3, 6.1 Hz), 7.13–7.29 (5H, m), 7.70 (1H, d, J = 8.4 Hz), 7.84 (1H, t, J = 8.2 Hz), 8.28 (1H, d, J = 8.2 Hz), 8.34–8.36 (1H, m), 8.62 (1H, s), 13.04 (1H, br); ^{13}C NMR (100 MHz, DMSO-d_6) δ 20.67, 101.39, 110.94, 113.39, 113.71, 115.71, 119.85, 123.29, 129.39, 131.69, 133.78, 138.41, 141.06, 142.61, 148.46, 148.84, 151.54, 154.91, 160.38, 163.20; IR (KBr): 3421, 1676, 1593, 1551, 1437 cm^{-1}; MS (EI): m/z 371 (M$^+$); HRMS: Calcd for $C_{22}H_{17}N_3O_3$ 371.1270. Found 371.1273.

4.1.2.4. 2-(4-Bromophenylimino)-7-hydroxy-2*H*-chromene-3-carboxylic acid pyridin-2-ylamide (5d: R = Br). Yield: 49%; mp: >300 °C; ^{1}H NMR (400 MHz, DMSO-d_6) δ 6.56 (1H, s), 6.78 (1H, d, J = 8.4 Hz), 7.15 (1H, t, J = 7.5 Hz), 7.31 (2H, d, J = 8.7 Hz), 7.60 (2H, d, J = 8.7 Hz), 7.72 (1H, d, J = 8.4 Hz), 7.85 (1H, t, J = 7.5 Hz), 8.28 (1H, d, J = 7.5 Hz), 8.32–8.34 (1H, m), 8.67 (1H, s), 12.80 (1H, br); ^{13}C NMR (100 MHz, DMSO-d_6) δ 101.45, 111.00, 113.60, 113.71, 115.53, 116.70, 119.92, 125.45, 131.78, 138.44, 143.21, 143.29, 148.44, 149.83, 149.85, 151.45, 154.84, 160.25, 163.32; IR (KBr): 3317, 1682, 1558, 1435 cm^{-1}; MS (EI): m/z 435 (M$^+$); HRMS: Calcd for $C_{21}H_{14}BrN_3O_3$ 435.0219. Found 435.0226.

4.1.2.5. 7-Hydroxy-2-(4-iodophenylimino)-2*H*-chromene-3-carboxylic acid pyridin-2-ylamide (5e: R = I). Yield: 60%; mp: >300 °C; ^{1}H NMR (400 MHz, DMSO-d_6) δ 6.55(1H, s), 6.78 (1H, dd, J = 2.2, 6.3 Hz), 7.13–7.18 (3H, m), 7.71–7.77 (3H, m), 7.84 (1H, t, J = 8.1 Hz), 8.27 (1H, d, J = 8.1 Hz), 8.32–8.34 (1H, m), 8.66 (1H, s), 12.79 (1H, br); ^{13}C NMR (100 MHz, DMSO-d_6) δ 100.11, 101.46, 111.12, 113.60, 113.72, 115.56, 119.91, 125.72, 131.80, 137.65, 138.46, 143.28, 143.66, 148.45, 149.79, 151.45, 154.85, 160.27, 163.33; IR (KBr): 3442, 1686, 1595, 1541, 1435 cm^{-1}; MS (EI): m/z 483 (M$^+$); HRMS: Calcd for $C_{21}H_{14}IN_3O_3$ 483.0080. Found 483.0074.

4.1.2.6. {4-[7-Hydroxy-3-(pyridin-2-ylcarbamoyl)chromen-2-ylideneamino]phenyl}-acetic acid (5f: R = CH_2CO_2H). Yield: 61%; mp: >300 °C; ^{1}H NMR (400 MHz, DMSO-d_6) δ 3.57 (2H, s), 6.51 (1H, s), 6.73 (1H, d, J = 8.7 Hz), 7.14 (1H, t, J = 7.3 Hz), 7.28–7.32 (4H, m), 7.67 (1H, d, J = 8.7 Hz), 7.83 (1H, t, J = 7.3 Hz), 8.27 (1H, d, J = 7.3 Hz), 8.33–8.35 (1H, m), 8.62 (1H, s), 13.00 (1H, br); ^{13}C NMR (100 MHz, DMSO-d_6) δ 40.92, 48.63, 101.52, 110.69, 113.71, 115.26, 119.81, 123.13, 129.90, 131.69, 131.79, 138.39, 142.15, 142.82, 148.46, 149.16, 151.57, 155.01, 160.42, 163.94, 173.34; IR (KBr): 3402, 1668, 1543, 1437, 1229 cm^{-1}; MS (EI): m/z 415 (M$^+$); HRMS: Calcd for $C_{23}H_{17}N_3O_5$ 415.1168. Found 415.1172.

4.1.2.7. 7-Hydroxy-2-phenylimino-2*H*-chromene-3-carboxylic acid pyridin-2-ylamide (5g: R = H). Yield: 52%; mp: 294–295 °C; ^{1}H NMR (400 MHz, DMSO-d_6) δ 6.51 (1H, s), 6.76 (1H, dd, J = 2.4, 6.2 Hz), 7.13–7.21 (2H, m), 7.32–7.46 (4H, m), 7.70 (1H, d, J = 8.6 Hz), 7.86 (1H, t, J = 8.0 Hz), 8.29 (1H, d, J = 8.0 Hz), 8.32–8.34 (1H, m), 8.65 (1H, s); ^{13}C NMR (100 MHz, DMSO-d_6) δ 101.38, 110.86, 113.50, 113.71, 115.49, 119.80, 123.15, 124.52, 128.88, 131.68, 138.44, 142.95, 143.84, 148.32, 149.28, 151.52, 154.90, 160.34, 163.40; IR (KBr): 3442, 1684, 1582, 1541, 1437 cm^{-1}; MS (EI): m/z 357 (M$^+$); HRMS: Calcd for $C_{21}H_{15}N_3O_3$ 357.1113. Found 357.1110.

4.1.2.8. 7-Hydroxy-2-(4-methoxyphenylimino)-2*H*-chromene-3-carboxylic acid iso-propylamide (5h: R_1 = *i*-Pr). Yield: 46%; mp: 229–231 °C; ^{1}H NMR (400 MHz, DMSO-d_6) δ 1.18 (6H, d, J = 6.6 Hz), 3.99 (1H, sept, J = 6.6 Hz), 6.55 (1H, s), 6.71 (1H, d, J = 8.3 Hz), 6.94 (2H, d, J = 8.5 Hz), 7.30 (2H, d, J = 8.5 Hz), 7.58 (1H, d, J = 8.3 Hz), 8.37 (1H, s), 10.18 (1H, d, J = 6.8 Hz), 10.72 (1H, br); ^{13}C NMR (100 MHz, DMSO-d_6) δ 22.35, 22.45, 55.21, 101.33, 111.01, 112.97, 114.05, 116.84, 124.88, 131.08, 136.79, 140.51, 148.14, 154.56, 156.36, 160.74, 162.34; IR (KBr): 3321, 1655, 1570, 1558, 1506, 1246 cm^{-1}; MS (EI): m/z 352 (M$^+$); HRMS: Calcd for $C_{20}H_{20}N_2O_4$ 352.1423. Found 352.1426.

4.1.2.9. 7-Hydroxy-2-(4-methoxyphenylimino)-2*H*-chromene-3-carboxylic acid butyl-amide (5i: R_1 = *n*-Bu). Yield: 40%; mp: 257–259 °C; ^{1}H NMR (400 MHz, DMSO-d_6) δ 0.89 (3H, t, J = 7.1 Hz), 1.33 (2H, sext, J = 7.1 Hz), 1.49 (2H, quint, J = 7.1 Hz), 3.35 (2H, t, J = 7.1 Hz), 3.74 (3H, s), 6.51 (1H, s), 6.70 (1H, d, J = 8.1 Hz), 6.93 (2H, d, J = 8.9 Hz), 7.26 (2H, d, J = 8.9 Hz), 7.56 (1H, d, J = 8.1 Hz), 8.35 (1H, s), 10.15 (1H, d, J = 5.1 Hz), 10.64 (1H, br); ^{13}C NMR (100 MHz, DMSO-d_6) δ 13.56, 19.71, 30.98, 55.13, 55.19, 101.29, 110.97, 112.90, 113.93, 114.00, 116.86, 124.72, 131.00, 136.91, 140.50, 148.21, 154.52, 156.25, 161.53, 162.27, 164.80; IR (KBr): 3373, 1665, 1570, 1504, 1246 cm^{-1}; MS (EI): m/z 366 (M$^+$); HRMS: Calcd for $C_{21}H_{22}N_2O_4$ 366.1580. Found 366.1585.

4.1.2.10. 7-Hydroxy-2-(4-methoxphenylino)-2*H*-chromene-3-carboxylic acid isobutyl-amide (5j: R_1 = *i*-Bu). Yield: 62%; mp: >300 °C; ^{1}H NMR (400 MHz, DMSO-d_6) δ 0.94 (6H, d, J = 6.6 Hz), 1.81 (1H, m), 2.08 (2H, d, J = 6.6 Hz), 3.77 (3H, s), 6.54 (1H, s), 6.72 (1H, d, J = 8.7 Hz), 6.95 (2H, d, J = 7.7 Hz), 7.28 (2H, d, J = 7.7 Hz), 7.60 (1H, d, J = 8.7 Hz), 8.39 (1H, s), 10.25 (1H, br); ^{13}C NMR (100 MHz, DMSO-d_6) δ 20.12, 27.99, 30.71, 46.35, 55.22, 101.34, 110.83, 113.15, 114.06, 116.67, 124.66, 131.12, 136.95, 140.72, 148.46, 154.61, 156.28, 161.70, 162.76; IR (KBr): 3420, 1663, 1558, 1506, 1244 cm^{-1}; MS (EI): m/z 366 (M^+); HRMS: Calcd for $C_{21}H_{22}N_2O_4$ 366.1580. Found 366.1584.

4.1.2.11. 7-Hydroxy-2-(4-methoxy-phenylimino)-2*H*-chromene-3-carboxylic acid cyclohexylamide (5k: R_1 = *c*-Hex). Yield: 63%; mp: 240–242 °C; ^{1}H NMR (400 MHz, DMSO-d_6) δ 1.31–1.84 (10H, m), 3.76 (3H, s), 3.79–3.81 (1H, m), 6.54 (1H, s), 6.71 (1H, dd, J = 2.2, 6.3 Hz), 6.95 (2H, d, J = 9.1 Hz), 7.29 (2H, d, J = 9.1 Hz), 7.59 (1H, d, J = 8.5 Hz), 8.38 (1H, s). 10.32 (1H, d, J = 7.8 Hz), 10.67 (1H, br); ^{13}C NMR (100 MHz, DMSO-d_6) δ 23.81, 25.22, 32.45, 55.22, 101.32, 111.04, 112.98, 114.09, 116.88, 124.81, 131.11, 136.79, 140.62, 148.28, 154.55, 156.35, 160.59, 162.33; IR (KBr): 3450, 1653, 1558, 1506 cm^{-1}; MS (EI): m/z 392 (M^+); HRMS: Calcd for $C_{23}H_{24}N_2O_4$ 392.1736. Found 392.1740.

4.1.2.12. 7-Hydroxy-2-(4-methoxyphenylimino)-2*H*-chromene-3-carboxylic acid (2-hydroxyethyl)amide (5l: $R_1 = (CH_2)_2$ OH). Yield: 80%; mp: 213–214 °C; ^{1}H NMR (400 MHz, DMSO-d_6) δ 3.39 (2H, t, J = 5.2 Hz), 3.54 (2H, t, J = 5.2 Hz), 3.77 (3H, s), 4.86 (1H, br), 6.56 (1H, s), 6.71 (1H, dd, J = 2.2, 6.1 Hz), 6.94 (2H, d, J = 9.0 Hz), 7.37 (2H, d, J = 9.0 Hz), 7.60 (1H, d, J = 8.3 Hz), 8.40 (1H, s), 10.41 (1H, br); ^{13}C NMR (100 MHz, DMSO-d_6) δ 41.75, 55.19, 59.73, 101.33, 110.99, 112.92, 113.91, 116.97, 125.15, 131.08, 136.81, 140.49, 147.77, 154.59, 156.33, 161.70, 162.30; IR (KBr): 3368, 1661, 1559, 1506 cm^{-1}; MS (EI): m/z 354 (M^+); HRMS: Calcd for $C_{19}H_{18}N_2O_5$ 354.1216. Found 354.1213.

4.1.2.13. 7-Hydroxy-2-(4-methoxyphenylimino)-2*H*-chromene-3-carboxylic acid (3-hydroxypropyl)amide (5m: $R_1 = (CH_2)_3$-OH). Yield: 72%; mp: 229–231 °C; ^{1}H NMR (400 MHz, DMSO-d_6) δ 1.67 (2H, quint, J = 6.6 Hz), 3.38 (2H, d, J = 6.6 Hz), 3.51 (2H, d, J = 6.6 Hz), 3.77 (3H, s), 4.56 (1H, br), 6.53 (1H, s), 6.71 (1H, dd, J = 2.3, 6.2 Hz), 6.95 (2H, d, J = 6.7 Hz), 7.32 (2H, d, J = 6.7 Hz), 7.60 (1H, d, J = 8.5 Hz), 8.39 (1H, s), 10.188 (1H, t, J = 5.6 Hz); ^{13}C NMR (100 MHz, DMSO-d_6) δ 32.11, 36.21, 55.16, 58.53, 101.29, 110.98, 112.91, 113.92, 113.94, 116.88, 124.83, 131.04, 136.93, 140.09, 148.09, 154.54, 156.25, 161.70, 162.28; IR (KBr): 3371, 1665, 1570, 1504, 1242 cm^{-1}; MS (EI): m/z 368 (M^+); HRMS: Calcd for $C_{20}H_{20}N_2O_5$ 368.1372. Found 368.1371.

4.1.2.14. 7-Hydroxy-2-(4-methoxyphenylimino)-2*H*-chromene-3-carboxylic acid benzylamide (5n: R_1 = Bn). Yield: 40%; mp: 257–259 °C; ^{1}H NMR (400 MHz, DMSO-d_6) δ 3.75 (3H, s), 4.55 (2H, d, J = 5.9 Hz), 6.52 (1H, s), 6.71 (1H, dd, J = 2.2, 6.2 Hz), 6.91–6.93 (2H, m), 7.24–7.26 (3H, m), 7.32–7.36 (4H, m), 7.61 (1H, d, J = 8.4 Hz), 8.42 (1H, s), 10.55 (1H, t, J = 5.9 Hz); ^{13}C NMR (100 MHz, DMSO-d_6) δ 42.78, 55.20, 101.35, 110.93, 113.06, 113.96, 116.74, 124.81, 126.95, 127.25, 128.48, 131.17, 136.86, 139.07, 140.86, 148.21, 154.66, 156.28, 161.92, 162.58; IR (KBr): 3407, 1661, 1558, 1506 cm^{-1}; MS (EI): m/z 400 (M^+); HRMS: Calcd for $C_{24}H_{20}N_2O_4$ 400.1423. Found 400.1426.

4.1.2.15. 8-Hydroxy-2-(4-methoxy-phenylimino)-2*H*-chromene-3-carboxylic acid pyridin-2-ylamide (5o: R_1 = OH, R_2 = H, R_3 = H). Yield: 88%; mp: 253–255 °C; ^{1}H NMR (400 MHz, DMSO-d_6) δ 3.80 (3H, s), 7.02 (2H, d, J = 8.9 Hz), 7.12–7.19 (3H, m), 7.27 (1H, d, J = 6.6 Hz), 7.75 (2H, d, J = 8.9 Hz), 7.87 (1H, t, J = 7.9 Hz), 8.41 (1H, d, J = 7.9 Hz), 8.41–8.43 (1H, m), 8.59 (1H, s), 13.48 (1H, br); ^{13}C NMR (100 MHz, DMSO-d_6) δ 55.26, 113.73, 114.05, 119.62, 119.66, 119.85, 119.98, 120.55, 124.60, 126.36, 135.96, 138.46, 141.54, 141.57, 144.37, 147.10, 148.60, 151.51, 153.14, 157.01, 159.99; IR (KBr): 3369, 1678, 1601, 1506, 1435 cm^{-1}; MS (EI): m/z 387 (M^+); HRMS: Calcd for $C_{22}H_{17}N_3O_4$ 387.1219. Found 387.1214.

4.1.2.16. 6-Hydroxy-2-(4-methoxy-phenylimino)-2*H*-chromene-3-carboxylic acid pyridin-2-ylamide (5p: R_1, R_3 = H, R_2 = OH). Yield: 59%; mp:>300 °C; ^{1}H NMR (400 MHz, DMSO-d_6) δ 3.79 (3H, s), 6.99–7.04 (3H, m), 7.15–7.18 (3H, m), 7.45 (2H, d, J = 8.9 Hz), 7.87 (1H, t, J = 8.1 Hz), 8.28 (1H, d, J = 8.1 Hz), 8.37–8.39 (1H, m), 8.60 (1H, s), 9.80 (1H, br); ^{13}C NMR (100 MHz, DMSO-d_6) δ 55.24, 113.77, 114.15, 114.27, 116.15, 119.14, 120.02, 120.52, 121.11, 125.14, 136.38, 138.49, 141.73, 146.30, 148.18, 148.55, 151.45, 153.96, 156.63, 160.03; IR (KBr): 3312, 1661, 1574, 1506 cm^{-1}; MS (EI): m/z 387 (M^+); HRMS: Calcd for $C_{22}H_{17}N_3O_4$. Found 387.1214.

4.1.2.17. 5-Hydroxy-2-(4-methoxy-phenylimino)-2*H*-chromene-3-carboxylic acid pyridin-2-ylamide (5q: R_1, R_2 = H, R_3 = OH). Yield: 49%; mp: 294–296 °C; ^{1}H NMR (400 MHz, DMSO-d_6) δ 3.79 (3H, s), 6.71 (1H, d, J = 8.6 Hz), 6.74 (1H, d, J = 8.6 Hz), 7.01 (2H, d, J = 8.8 Hz), 7.16 (1H, t, J = 7.3 Hz), 7.39–7.45 (3H, m), 7.86 (1H, t, J = 7.3 Hz), 8.28 (1H, d, J = 7.3 Hz), 8.36–8.38 (1H, m), 8.75 (1H, s); ^{13}C NMR (100 MHz, DMSO-d_6) δ 55.22, 105.66, 107.98, 110.57, 113.73, 114.13, 117.86, 119.94, 125.09, 134.38, 136.28, 136.61, 138.45, 147.79, 148.52, 151.46, 153.82, 156.09, 156.65, 160.09; IR (KBr): 3319, 1684, 1541, 1506 cm^{-1}; MS (EI): m/z 387 (M^+); HRMS: Calcd for $C_{22}H_{17}N_3O_4$ 387.1219. Found 387.1221.

4.1.2.18. 2-(4-Methoxy-phenylimino)-2*H*-chromene-3-carboxylic acid pyridin-2-ylamide (5r: R_1, R_2, R_3 = H). Yield: 75%; mp: 249–250 °C; ^{1}H NMR (400 MHz, DMSO-d_6) δ 3.83 (3H, s), 6.94 (2H, d, J = 9.0 Hz), 7.03 (1H, t, J = 6.7 Hz), 7.14–7.24 (2H, m), 7.45–7.52 (4H, m), 7.72 (1H, t, J = 6.7 Hz), 8.32–8.34 (2H, m). 8.56 (1H, s), 13.25 (1H, br); ^{13}C NMR (100 MHz, DMSO-d_6) δ 55.46, 114.00, 114.78, 115.47, 119.07, 119.75, 121.47, 124.45, 125.55, 129.43, 132.85, 136.56, 137.80, 141.15, 147.42, 148.38, 151.89, 153.55, 157.17, 160.56; IR (KBr): 1676, 1541, 1506, 1437 cm^{-1}; MS (EI): m/z 371 (M^+); HRMS: Calcd for $C_{22}H_{17}N_3O_3$ 371.1270. Found 371.1271.

4.2. Biological assays

4.2.1. Preparation of recombinant enzymes

Recombinant AKR1B1[22] and AKR1B10 with the N-terminal 6-His tag,[14] and Trp220Tyr and Gln303Ser mutant AKR1B10s[23] were expressed in *Escherichia coli* cells harboring their cDNAs, and purified to homogeneity, as described previously.

4.2.2. Assay of enzyme activity

The reductase and dehydrogenase activities of the enzymes were determined at 25 °C by measuring the rate of change in NADPH absorbance (at 340 nm) and fluorescence (at 455 nm with an excitation wavelength of 340 nm), respectively.[14] The IC_{50} values for inhibitors were determined in the reaction mixture that consisted of 0.1 M potassium phosphate, pH 7.4, 0.1 mM NADPH, 0.2 mM pyridine-3-aldehyde (approximately 15 × K_m concentration), and enzyme, in a total volume of 2.0 mL. The inhibitor constant, K_i, for **5n** was determined by kinetic analysis in the $NADP^+$-linked geraniol oxidation, because the reaction of AKR1B10 follows an order bi bi mechanism[14] and many competitive inhibitors including **1** show mixed-type or noncompetitive

inhibition with respect to pyridine-3-aldehyde in the reduction reaction.[10,11,13,14,17,18] The K_i value was estimated from the replots of the slopes and intercepts of double reciprocal plot of the five geraniol concentrations versus velocities, which were determined in the presence of a saturating $NADP^+$ concentration (0.25 mM) and three concentrations of the inhibitor. The IC_{50} and K_i values are expressed as the means of at least three determinations.

4.2.3. Molecular modeling and energy minimization

The coordinates for AKR1B10 (PDB code: 1ZUA)[24] were obtained from the RCSB Protein Data Bank. The structure was prepared using the Maestro (Schrödinger, LLC, Portland, OR) software package Version 8.5, as described previously.[14] The docking calculations were performed using the program Glide 5.043 on a Linux workstation under the conditions described previously.[14] The docked models shown in Figure 1 were generated using PyMOL (DeLano Scientific, San Carlos, CA, USA).

Acknowledgement

This work is supported in part by JSPS Grant-in-Aid for Young Scientists (B) from the Japan Society for the Promotion of Science Grant Number 24790114.

References and notes

1. Cao, D.; Fan, S. T.; Chung, S. S. *J. Biol. Chem.* **1998**, *273*, 11429.
2. Fukumoto, S.; Yamauchi, N.; Moriguchi, H.; Hippo, Y.; Watanabe, A.; Shibahara, J.; Taniguchi, H.; Ishikawa, S.; Ito, H.; Yamamoto, S.; Iwanari, H.; Hironaka, M.; Ishikawa, Y.; Niki, T.; Sohara, Y.; Kodama, T.; Nishimura, M.; Fukayama, M.; Dosaka-Akita, H.; Aburatani, H. *Clin. Cancer Res.* **2005**, *11*, 1776.
3. Yoshitake, H.; Takahashi, M.; Ishikawa, H.; Nojima, M.; Iwanari, H.; Watanabe, A.; Aburatani, H.; Yoshida, K.; Ishi, K.; Takamori, K.; Ogawa, H.; Hamakubo, T.; Kodama, T.; Araki, Y. *Int. J. Gynecol. Cancer* **2007**, *17*, 1300.
4. Heringlake, S.; Hofdmann, M.; Fiebeler, A.; Manns, M. P.; Schmiegel, W.; Tannapfel, A. *J. Hepatol.* **2010**, *52*, 220.
5. Chung, Y. T.; Matkowskyj, K. A.; Li, H.; Bai, H.; Zhang, W.; Tsao, M. S.; Liao, J.; Yang, G. Y. *Mod. Pathol.* **2012**, *25*, 758.
6. Ma, J.; Luo, D. X.; Huang, C.; Shen, Y.; Bu, Y.; Markwell, S.; Gao, J.; Liu, J.; Zu, X.; Cao, Z.; Gao, Z.; Lu, F.; Liao, D. F.; Cao, D. *Int. J. Cancer* **2012**, *131*, 862.
7. Yan, R.; Zu, X.; Ma, J.; Liu, Z.; Adeyanju, M.; Cao, D. *Int. J. Cancer* **2007**, *121*, 2301.
8. Wang, C.; Yan, R.; Luo, D.; Watabe, K.; Liao, D. F.; Cao, D. *J. Biol. Chem.* **2009**, *284*, 26742.
9. Satow, R.; Shitashige, M.; Kanai, Y.; Takeshita, F.; Ojima, H.; Jigami, T.; Honda, K.; Kosuge, T.; Ochiya, T.; Hirohashi, S.; Yamada, T. *Clin. Cancer Res.* **2010**, *16*, 2518.
10. Soda, M.; Hu, D.; Endo, S.; Takemura, M.; Li, J.; Wada, R.; Ifuku, S.; Zhao, H. T.; El-Kabbani, O.; Ohta, S.; Yamamura, K.; Toyooka, N.; Hara, A.; Matsunaga, T. *Eur. J. Med. Chem.* **2012**, *48*, 321.
11. Matsunaga, T.; Wada, Y.; Endo, S.; Soda, M.; El-Kabbani, O.; Hara, A. *Front. Pharmacol.* **2012**, *3*, 5.
12. Matsunaga, T.; Yamane, Y.; Iida, K.; Endo, S.; Banno, Y.; El-Kabbani, O.; Hara, A. *Anticancer Drugs* **2011**, *22*, 402.
13. Crosas, B.; Hyndman, D. J.; Gallego, O.; Martras, S.; Pares, X.; Flynn, T. G.; Farres, J. *Biochem. J.* **2003**, *373*, 973.
14. Endo, S.; Matsunaga, T.; Mamiya, H.; Ohta, C.; Soda, M.; Kitade, Y.; Tajima, K.; Zhao, H. T.; El-Kabbani, O.; Hara, A. *Arch. Biochem. Biophys.* **2009**, *487*, 1.
15. Li, H.; Yang, A. L.; Chung, Y. T.; Zhang., W.; Liao, J.; Yang, G. Y. *Carcinogenesis* **2013**, *34*, 2090.
16. Ma, J.; Yan, R.; Zu, X.; Cheng, J. M.; Rao, K.; Liao, D. F.; Cao, D. *J. Biol. Chem.* **2008**, *283*, 3418.
17. Matsunaga, T.; El-Kabbani, O.; Hara, A. In *Molecular Mechanisms of Tumor Cell Resistance to Chemotherapy*; Bonavida, B., Ed.; Springer: New York, 2013; pp 109–134.
18. Endo, S.; Matsunaga, T.; Kuwata, K.; Zhao, H. T.; El-Kabbani, O.; Kitade, Y.; Hara, A. *Bioorg. Med. Chem.* **2010**, *18*, 2485.
19. Baba, S. P.; Barski, O. A.; Ahmed, Y.; O'Toole, T. E.; Conklin, D. J.; Bhatnagar, A.; Srivastava, S. *Diabetes* **2009**, *58*, 2486.
20. Nagata, N.; Kusakari, Y.; Fukunishi, Y.; Inoue, T.; Urade, Y. *FEBS J.* **2011**, *278*, 1288.
21. Gorobets, N. Y.; Yousefi, B. H.; Belaj, F.; Kappe, C. O. *Tetrahedron* **2004**, *60*, 8633.
22. Iino, T.; Tabata, M.; Takikawa, S.; Sawada, H.; Shintaku, H.; Ishikura, S.; Hara, A. *Arch. Bichem. Biohys.* **2003**, *416*, 180.
23. Matsunaga, T.; Endo, S.; Soda, M.; Zhao, H. T.; El-Kabbani, O.; Tajima, K.; Hara, A. *Biochem. Biophys. Res. Commun.* **2009**, *389*, 128.
24. Gallego, O.; Ruiz, F. X.; Ardevol, A.; Dominguez, M.; Alvarez, R.; de Lera, A. R.; Rovira, C.; Farres, J.; Fita, I.; Pares, X. *Proc. Natl. Acad. Sci. U.S.A.* **2007**, *104*, 20764.

BIOCHEMISTRY
including biophysical chemistry & molecular biology

Article

pubs.acs.org/biochemistry

Nearly Reversible Conformational Change of Amyloid Fibrils as Revealed by pH-Jump Experiments

Kei-ichi Yamaguchi,[†,‡] Yuji O. Kamatari,[‡,§] Mayuko Fukuoka,[†,‡] Reiji Miyaji,[¶] and Kazuo Kuwata*[,†,‡]

[†]United Graduate School of Drug Discovery and Medical Information Sciences, [‡]Center for Emerging Infectious Diseases, [§]Life Science Research Center, and [¶]Supporting and Development Center for Technology Education, Faculty of Engineering, Gifu University, Yanagido 1-1, Gifu 501-1193, Japan

Supporting Information

ABSTRACT: pH-jump induced conformational transitions between substates of preformed amyloid fibrils made by a fragmented peptide of helix 2 (H2 peptide) of MoPrP were detected, and their kinetics were analyzed using a novel pH-jump apparatus specially designed for observing amyloids. Previously, we reported that H2 peptide formed ordered fibrils with a minimum at 207 nm on CD spectra at pH 2.9 (named pH 2.9 fibrils), but formed aggregate-like fibrils with a minimum at 220 nm at pH 7.5 (named pH 7.5 fibrils). When pH-jump from 2.9 to 7.5 was performed, the CD spectrum changed instantly, but the finally observed ellipticities were clearly distinct from those of pH 7.5 fibrils. Thus, the finally observed state is termed 'pH 7.5-like fibrils'. However, pH 7.5-like fibrils reverted to the conformation very similar to that of the pH 2.9 fibrils when the pH of the solution was restored to 2.9. Then, we examined the kinetics of the nearly reversible conformational changes between pH 2.9 fibrils and pH 7.5-like fibrils using ANS fluorescence stopped-flow, and we observed relatively fast phases (0.7−18 s^{-1}). In contrast, the conversion between pH 7.5-like fibrils and pH 7.5 fibrils never occurred (<0.2 day^{-1}). Thus, H2 fibrils can be switched readily between distinct conformations separated by a low energy barrier, while a large energy barrier clearly separated the different conformations. These conformational varieties of amyloid fibrils may explain the physical basis of the diversity in prion.

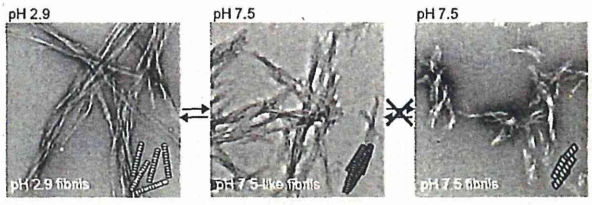

Amyloid fibrils may be associated with many neurodegenerative diseases such as Alzheimer's, Parkinson's, and prion diseases.[1−4] Prion diseases are a group of fatal neurodegenerative diseases, including Creutzfeldt-Jakob disease (CJD) and kuru in humans, as well as scrapie and bovine spongiform encephalopathy (BSE) in animals. Prion diseases emerged as a major public issue following epidemics of BSE, which crossed the species barrier to cause variant CJD in humans.[5,6] Pathogenesis of these unusual diseases is associated with the conformational rearrangement of a cellular isoform of prion protein (PrP^C) to a scrapie isoform (PrP^{Sc}) in the brain.[3,7,8] While PrP^C is monomeric and rich in α-helical structure,[9] the PrP^{Sc} conformer is characterized by an increased proportion of β-sheet structure and a propensity to aggregate into amyloid fibrils or plaques.[10]

The formation of multiple phenotypes of prion strains which are transmitted within the same or distinct species can be caused by the template-dependent polymerization reaction of PrP^{Sc}.[11−14] Mammalian prion amyloids from different species were shown to adopt distinct secondary structures and morphologies measured by Fourier transform infrared (FT-IR) and atomic force microscopy, respectively.[12] Importantly, cross-seeding of prion monomers from one species with preformed fibrils from another species produced a new amyloid strain that exhibits the secondary structure and morphology of the template fibrils.[12] Moreover, selective pressures result in the emergence of various mutants, and biologically cloned prion populations gradually become heterogeneous by accumulating mutants.[15] Prions may show the hallmarks of Darwinian evolution. Thus, conformational and morphological changes of amyloid fibrils formed from the same protein are one of the most intriguing aspects of amyloid studies,[16] because the fibril conformation, the fibril biological activity, and the toxicity might be correlated.

However, their high molecular weight and noncrystalline assembly preclude the use of conventional structural biological tools, such as X-ray crystallography or solution NMR, which are typically used for acquiring high-resolution structural information. Recently, it has been found that magic-angle-spinning solid-state NMR methods are suitable for use on amyloid fibrils, and can visualize atomic-level structure, in which β-strands are stacked in parallel and in register.[17−19] A report of the structure of a short amyloidogenic peptide, revealed by X-ray diffraction of a microcrystal, is consistent with this view.[20] In contrast, Knowles et al. reported that mature amyloid fibrils are stiffer than most functional intracellular biological filaments,[21] such as tubulin and actin filaments, and are stabilized mainly by an interbackbone hydrogen-bonding network and further modulated by variable side-chain interactions. Although conversion

Received: June 2, 2013
Revised: September 2, 2013
Published: September 3, 2013

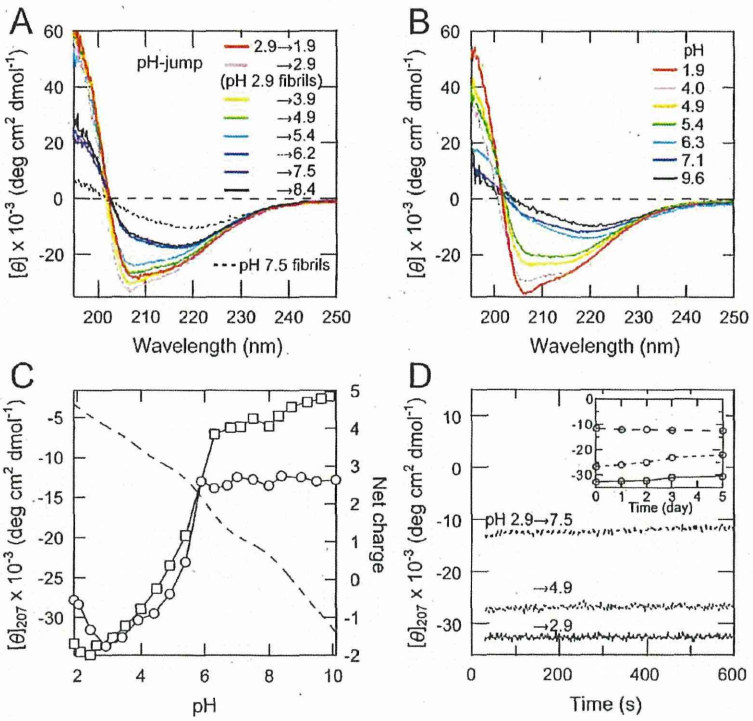

Figure 1. Single pH-jump experiments of H2 amyloid fibrils. (A) CD spectra of H2 fibrils after the pH-jump from 2.9 to various pH values (solid line) and that of pH 7.5 fibrils formed at pH 7.5 (dotted line). (B) CD spectra of H2 fibrils formed under various pH conditions after incubation for 2 days, taken from Yamaguchi et al.[26] (C) Conformational changes of H2 fibrils after the pH-jump from 2.9 to various pHs (○) and fibril formation of the H2 peptide under the various pH conditions (□) monitored as ellipticity at 207 nm. The net charge of the H2 peptide is indicated by a dashed line (right ordinate). (D) Conformational changes of H2 fibrils after a manual pH-jump, monitored as ellipticity at 207 nm with a dead time of 30 s. The inset shows the conformational changes of H2 fibrils after pH-jumps from 2.9 to 2.9 (solid line), 4.9 (dotted line), and 7.5 (dashed line) during incubation for 5 days at 25 °C.

from a native fold into the amyloid state is a complex process that involves several consecutive steps, including the initial formation of small oligomeric aggregates,[22,23] the conversion to the amyloid state represents the most conformationally rigid and thermodynamically stable folding.[2,21]

Previously, we reported that helix 2 region of mouse prion protein (MoPrP) (Figure S1 of the Supporting Information) was relatively hydrophobic and had a high propensity of β-sheet conformation among MoPrP, predicted by primary structure analyses using hydrophobicity scales[24] and ANTHEPROT,[25] respectively. We also reported a fragmented peptide of helix 2 (H2 peptide) formed ordered fibrils with a minimum in its circular dichroism (CD) spectrum at 207 nm at acidic pHs (Figure 1B), but aggregate-like fibrils with a minimum at 220 nm were formed at slightly basic pHs near the isotropic point (pI) of 8.6 (Figure 1B).[26] In addition, the recent studies indicate that the low pH solution is an ideal trigger of PrP^C to PrP^β conversion and PrP amyloid fibril formation.[27−29] Thus, the amyloid fibril formation is sensitive to the pH environment. In this study, to obtain insight into the mechanism of pH-dependent structural conversion of preformed amyloid fibrils, pH-jump experiments were performed using H2 fibrils. We found that the conformation of H2 fibrils dramatically changed after the pH-jump from 2.9 to 7.5. Surprisingly, the fibril conformation nearly reverted after restoration of the solution pH to 2.9, as shown by CD and FT-IR spectra, and electron microscope (EM) observations. Moreover, kinetic analyses using the newly designed stopped-flow system adapted for amyloid fibrils revealed that these conformational changes can occur quite rapidly after the pH-jumps. Here we discuss these findings regarding the unique energy profile of H2 fibrils.

■ MATERIALS AND METHODS

H2 Peptide and Amyloid Fibril Formation. The amino acid sequence of the H2 peptide is QNNFVHDCVNITIKQHTVTTTTK, corresponding to a helix 2 of MoPrP (Figure S1 of the Supporting Information).[9] The H2 peptide was synthesized with Fmoc chemistry using a PS-3 peptide synthesizer (Protein Technologies, Tucson, AZ). The cleaved peptides was purified (>95%) by reversed phase HPLC using a COSMOSIL $5C_{18}$-AR-II column (Nacalai Tesque, Tyoto, Japan). The molecular weight of the peptide was measured by matrix-assisted laser desorption ionization time-of-flight (MALDI-TOF) mass spectrometry (Bruker Daltonics, Billerica, MA). H2 amyloid fibrils were formed using a peptide concentration of 100 μM (0.26 mg/mL) in 25 mM Gly−HCl buffer (pH 2.9) containing 100 mM NaCl at 37 °C without agitation. After 1 day of incubation, the conformation of the H2 fibrils was monitored by far-UV CD spectroscopy.

pH-Jump Experiments of H2 Amyloid Fibrils. In single pH-jump experiments from 2.9 to various pH values, the solution of H2 fibrils in 25 mM Gly−HCl (pH 2.9) containing 100 mM NaCl was diluted 2.5-fold with various pH solutions containing 25 mM buffers and 100 mM NaCl, and the solution pH was confirmed using a Handy pH Meter (Horiba, Kyoto, Japan). The following buffers were used: Gly−HCl (pH 1.9−

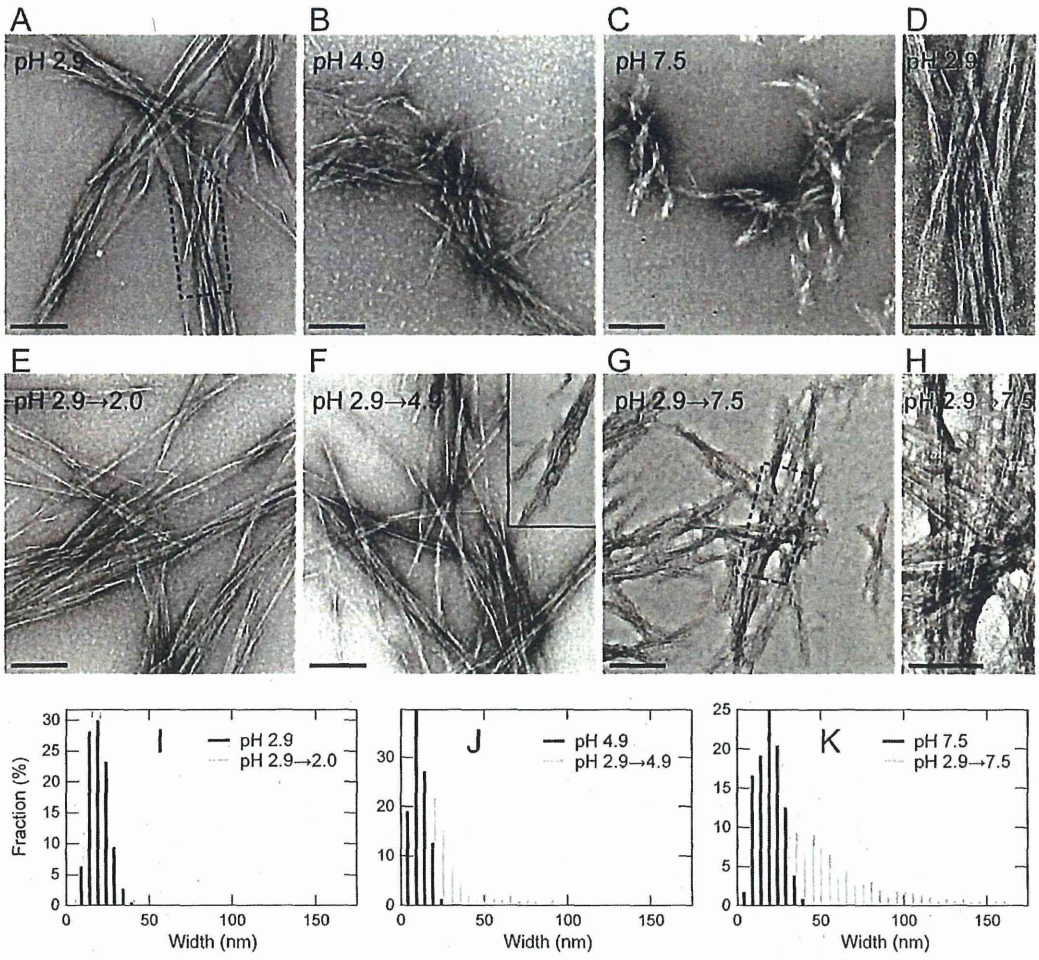

Figure 2. EM observations of H2 fibrils. (A)–(C) Amyloid fibrils prepared from the H2 peptide at pH 2.9 (A), 4.9 (B), and 7.5 (C) after 1 day of incubation. (E)–(G) H2 amyloid fibrils after the pH-jump from 2.9 to 2.0 (E), 4.9 (F), and 7.5 (G). The inset shows thick fibrils observed at other places after the pH-jump to 4.9. Scale bars = 200 nm. (D) and (H) Magnified images of H2 fibrils taken from panels (A) and (G), respectively. The magnified regions are indicated by the square. Scale bars = 100 nm. (I)–(K) Fibril width distribution of H2 fibrils formed at pH 2.9 (I, black bars), 4.9 (J, black bars), and 7.5 (K, black bars) before the pH-jump, and that of H2 fibrils after the pH-jump from 2.9 to 2.0 (I, gray bars), 4.9 (J, gray bars), and 7.5 (K, gray bars). Fibril widths of 230–410 fibrils were measured in each EM image, and the fraction (%) of each fibril width was plotted.

3.4), acetate–NaOH (pH 3.9–5.4), phosphate–NaOH (pH 5.9–7.0), Tris–HCl (pH 7.5–9.0), and Gly–NaOH (pH 9.5–10.1).

In double pH-jump experiments, first the H2 fibril solution at pH 2.9 was diluted 2.5-fold with 25 mM Tris–HCl containing 100 mM NaCl so that the solution pH was set to 7.5. After several times of incubation at 25 °C, the solution was diluted 2.5-fold again with 25 mM Gly–HCl containing 100 mM NaCl so that the solution pH was set to 2.9.

CD Measurement. Static far-UV CD spectra of H2 fibrils at various pH values were measured using a quartz cell with a light-path of 1 mm and a peptide concentration of 0.1 mg/mL at 25 °C on an AVIV model 215s spectropolarimeter (AVIV Biomedical, Lakewood, NJ). Kinetic far-UV CD spectra at 207 nm were measured at 25 °C after the pH-jumps, after manual mixing with a dead time of 30 s. The results are expressed as mean residue ellipticity $[\theta]$ (deg cm^2 dmol^{-1}).

EM Measurement. A 2-μL aliquot of sample solution was placed on a copper grid (400 mesh) covered with carbon film for 1 min, and excess solution was removed by blotting with filter paper. The grid was negatively stained with a 5-μL droplet of 2% uranyl acetate for 1 min. Again, the liquid on the grid was removed by blotting and dried. Electron micrographs were taken using a JEM-2100F transmission EM (JEOL, Tokyo, Japan), operating at 200 kV acceleration with a magnification of ×20,000.

Light Scattering Measurement and Precipitation Assay. Light scattering measurements of fibril solutions containing 0.05 mg/mL H2 fibrils, 25 mM buffers, and 100 mM NaCl at various pH values were performed with a Hitachi F-7000 fluorescence spectrophotometer at 25 °C. The wavelengths for excitation and emission were both set at 350 nm, and the slit length was 2.5 nm.

For precipitation assay, the solutions of H2 fibrils were centrifuged (30,000 × g at 4 °C for 1 h) to precipitate amyloid fibrils. The concentration of H2 peptide in supernatant was determined by UV absorption by applying the formula $(A_{215} - A_{225}) \times 144$ = protein concentration (μg/mL),[30] and the precipitated fraction was calculated by subtracting this value from the initial concentration of monomeric peptide.

FT-IR Measurement. FT-IR absorption spectra were recorded with a Bruker Tensor 27 FT-IR spectrometer (Bruker Optics, Billerica, MA) equipped with a liquid N_2-cooled mercury cadmium telluride (MCT) detector and a BioATR II unit. The fibril solutions were centrifuged (30,000 × *g* at 4 °C for 1 h) to precipitate the fibrils, and the precipitated fibrils were loaded onto the surface of a BioATR II prism. The spectra were recorded at 25 °C with a resolution of 2 cm^{-1} and were averaged for 128 scans. From the spectrum of each sample, a corresponding buffer spectrum was subtracted. Difference spectra were calculated by subtracting the spectrum of absorption derived from C=O stretching of amide I, in which the range 1585–1715 cm^{-1} was corrected so as to be equal between two samples.

Development of Stopped-Flow Instrument and ANS Fluorescence Measurement. Kinetic ANS fluorescence data were collected by using a stopped-flow instrument manufactured in-house in order to flow amyloid fibril solution including large aggregates. The mixer possessing a Y-shaped channel with a diameter of 0.75 mm was connected using a PEEK tube with a diameter of 1.0 mm. A Hitachi F-7000 fluorescence spectrophotometer with a flow-cell set to a volume of 0.44 mL was used. The sample in the syringe was applied using a 200 V motor (Toshiba, Tokyo, Japan). The rotational frequency was regulated using a TOSVERT VF-nC3 inverter (Toshiba, Tokyo, Japan) to adjust the flow speed of the solution. NATA fluorescence measurements were performed at 25 °C with wavelengths of excitation at 295 nm and emission at 350 nm. The final concentration of NATA was kept constant at 1.8 μM after the 1:11.6 mixing of various concentrations of NBS and 2 μM NATA solutions. The mixing dead time was determined to be 130 ms by measuring the fluorescence quenching reaction of NATA by NBS. The refolding reaction of βLG was induced by dilution of urea from a concentration of 7.0 to 0.6 M at pH 3.0, and was monitored by the intensity change of Trp fluorescence with wavelengths of excitation at 295 nm and emission at 350 nm. The final concentration of βLG was 7.9 μM after the 1:11.6 mixing of denatured βLG solution and refolding buffer.

Static fluorescence measurements of 1-anilinonaphthalene-8-sulfonic acid (ANS) bound to the H2 fibrils were performed with excitation at 360 nm and monitored at 400–600 nm on a Hitachi F-7000 fluorescence spectrophotometer (Hitachi High-Tech, Tokyo, Japan). The fluorescence of the fibril solutions containing 0.01 mg/mL H2 fibrils, 25 mM buffers, 100 mM NaCl, and 10 μM ANS at various pH values was measured at 25 °C. ANS fluorescence spectrum in the absence of protein was used as baseline. Stopped-flow ANS fluorescence measurements to monitor the conformational changes of H2 fibrils were performed at 25 °C with wavelengths of excitation at 360 nm and emission at 475 nm. The final concentration of the H2 fibrils was 0.01 mg/mL after the 1:11.6 mixing of the fibril solution and pH-jump buffer, both of which contained 25 mM buffers, 100 mM NaCl, and 10 μM ANS. The following buffers were used: Gly–HCl (pH 2.9) and Tris–HCl (pH 7.5). The solution pH after mixing was confirmed using a Handy pH Meter. Nonlinear least-squares fitting was performed with IGOR Pro software (WaveMetrics, Lake Oswego, OR).

RESULTS

Single pH-Jump Experiments of H2 Amyloid Fibrils. As reported previously, at pH 2.9 the H2 peptide forms ordered amyloid fibrils with a minimum at 207 nm and immensely large negative ellipticity (−33,600 deg cm^2 $dmol^{-1}$) (Figure 1A, pH 2.9 fibrils), but at pH 7.5 it forms disordered fibrils with a minimum at 220 nm (−9900 deg cm^2 $dmol^{-1}$) (Figure 1A, pH 7.5 fibrils).[26] Although the CD spectrum of H2 fibrils at pH 2.9 has a minimum at 207 nm (Figure 1A), it is not α-helix conformation but corresponds to an ordered β-sheet conformation of H2 amyloid fibrils, because their FT-IR spectrum and second derivative show only intermolecular β-sheet and β-turn conformations, as described below (Figure 5A,D, pH 2.9 fibrils). In addition, the similar CD spectra have also been reported by other amyloid fibrils forming the ordered β-sheet conformation.[31,32] Moreover, since the CD spectra of model cyclic peptides, forming β-turn conformations of type I or II′, showed a minimum around 205 nm,[33−35] the CD spectrum of H2 fibrils at pH 2.9 would be a combination of β-sheet and type I or II′ β-turn conformations of ordered amyloid fibrils.[26] EM observations showed that relatively long and ordered fibrils, which consisted of several protofilaments, were formed at pH 2.9 (Figure 2A), while short and aggregate-like fibrils were formed at pH 7.5 (Figure 2C). Thus, the H2 peptide formed distinct types of fibrils depending on pH, and the formation of the long and ordered fibrils would be formed by the moderate repulsion between peptides. Here, we will refer to the fibrils formed at pH 2.9 as 'pH 2.9 fibrils', and those formed at pH 7.5 as 'pH 7.5 fibrils'.

Initially, we monitored various spectroscopic parameters associated with the structural conversion of preformed amyloid fibrils induced by pH-jumps from 2.9 to various pHs, 1.9–9.9. The pH was changed by diluting 2.5-fold with buffers containing the same concentration of salt. The CD spectra of pH 2.9 fibrils changed instantly with the pH (Figure 1A). Although the CD spectrum after the pH-jump to 3.9 was similar to that seen at pH 2.9, the ellipticity at 207 nm gradually decreased as the solution pH increased (Figure 1A,C), and the minimum shifted from 207 to 218 nm at the jump to pH 7.5 (Figure 1A). After the pH-jump to 7.5, the CD spectrum showed a minimum at 218 nm with relatively small ellipticity (−17,200 deg cm^2 $dmol^{-1}$) (Figure 1A), which somewhat resembled those for pH 7.5 fibrils formed without jump. Here, we named the fibrils formed after the jump to pH 7.5 'pH 7.5-like fibrils'. However, the CD ellipticities at 207 nm after pH-jumps to pH 6 to approximately 10 were negatively larger than those of fibrils formed at the same pH at equilibrium (Figure 1C). Thus, it appears that the pH 7.5-like fibrils partially retain the conformation of pH 2.9 fibrils, even after jumping to pH 7.5. After the pH-jump to pH 1.9, which is very acidic, ellipticity also decreased, but imperfectly returned to the level of fibrils formed at pH 1.9 at equilibrium (Figure 1A,C), suggesting hysteresis or large barriers between pH 2.9 fibrils and other fibrils formed at equilibrium.

Previously, we reported that two different types of amyloid fibrils are formed, depending on pH, and that the midpoint of the transition is approximately pH 5 (Figure 1C, □).[26] The midpoint of the conformational transition of fibrils following the pH jump also occurred at approximately pH 5 (Figure 1C, ○). Thus, the conformational changes of preformed H2 fibrils induced by the pH-jump were highly sensitive to the pH of the final solution, similar to the process of fibril formation from the monomeric peptide. Importantly, the conformational changes induced by manual pH-jumps from 2.9 to 4.5 or 7.5 were completed within the dead time of 30 s (Figure 1D), and these conformations were stable for at least 5 days (Figure 1D, inset). Since amyloid fibril formation of the H2 peptide requires at

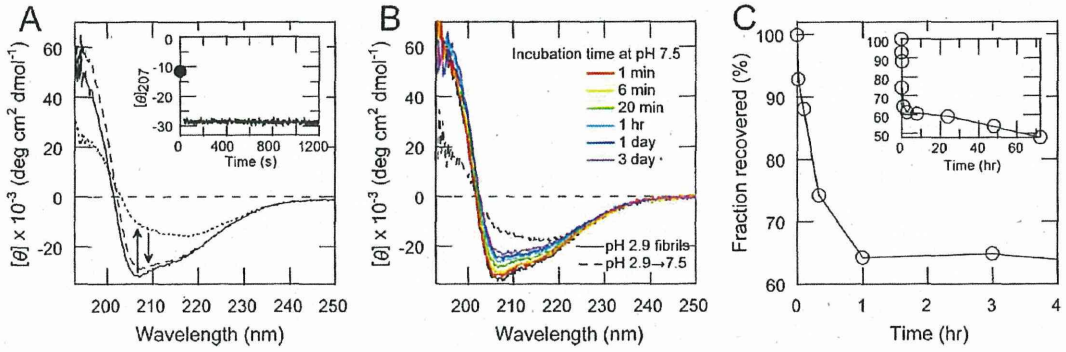

Figure 3. Conformational changes of H2 fibrils after the double pH-jump. (A) CD spectra of pH 2.9 fibrils before the pH-jump (solid line) and after a single pH-jump from 2.9 to 7.5 (dotted line), and a double pH-jump, pH 2.9 → 7.5 → 2.9 (dashed line). The inset shows the conformational changes of H2 fibrils after the double pH-jump, monitored as ellipticity at 207 nm. The ellipticity of H2 fibrils after the single pH-jump to 7.5 is shown by the closed circle. (B) CD spectra of H2 fibrils after incubation at pH 7.5 and 25 °C in the double pH-jump. The incubation times at pH 7.5 are depicted in the figure. CD spectra of H2 fibrils before the pH-jump at pH 2.9 (black solid line) and after the single pH-jump from 2.9 to 7.5 (black dashed line) are overlapped. (C) Incubation time-dependence at pH 7.5 in the double pH-jump experiment. The fraction recovered was estimated from the ellipticity at 207 nm. The inset shows the incubation time-dependence during 3 days of incubation.

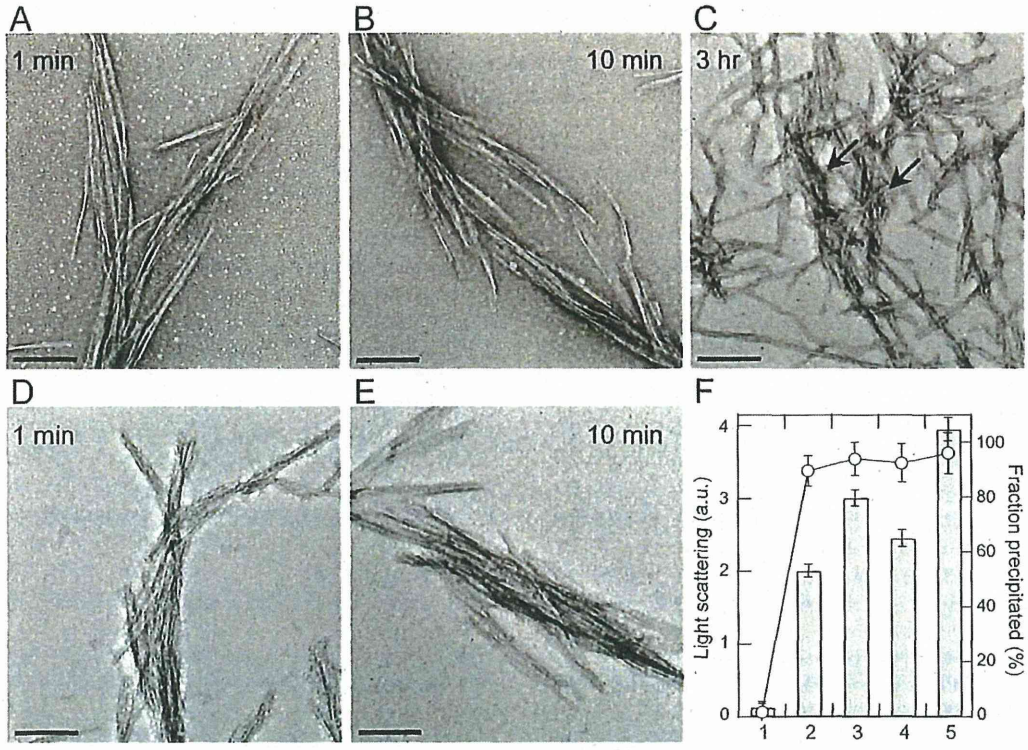

Figure 4. H2 amyloid fibrils after double pH-jump experiments. (A)–(E) EM images of H2 fibrils after incubation for 1 min (A,D), 10 min (B,E), and 3 h (C) at pH 7.5 and 25 °C in the double pH-jump. Thin fibrils (A,B) and thick fibrils (D,E), both types of fibrils (C) were observed. Thick fibrils are indicated by arrow (C). Scale bars are 200 nm. (F) Light scattering measurements (left ordinate, bar) and precipitated fraction (right ordinate, cycle) of H2 peptide monomer (1), and H2 fibrils before the pH-jump of pH 2.9 fibrils (2) and after a single pH-jump from 2.9 to 7.5 (3) and a double pH-jump pH 2.9 → 7.5 → 2.9 after incubation for 10 min at pH 7.5 (4), and pH 7.5 fibrils (5). The measurements were repeated three times.

least 3–4 h at 37 °C,[26] these conformational changes induced by the pH-jumps occurred directly, without involving the dissociation and subsequent aggregation process.

EM observations and fibril width distribution of H2 fibrils showed that after the pH-jump from 2.9 to 2.0, relatively long and thin amyloid fibrils with a diameter of 15–25 nm were observed (Figure 2E and I, gray), and their morphology and width were similar to those of pH 2.9 fibrils before the pH-jump (Figure 2A and I, black). After the pH-jump to 4.9, thin fibrils with a diameter of 15–20 nm (Figure 2F), which were ordered rather than those observed in the formation of fibrils from the monomer at pH 4.9 (Figure 2B), and a small number of thick fibrils were formed (Figure 2F, inset, and J, gray). After the pH-jump to 7.5, thick fibrils with a diameter of >50 nm